

Calculations of positron lifetimes in a jog and vacancies on an edge-dislocation line in Fe

Yasushi Kamimura

Department of High Energy Engineering Science, Interdisciplinary Graduate School of Engineering Sciences, Kyushu University, 6-1 Kasuga-koen, Kasuga, Fukuoka 816, Japan

Tetsuo Tsutsumi and Eiichi Kuramoto

Research Institute for Applied Mechanics, Kyushu University, 6-1 Kasuga-koen, Kasuga, Fukuoka 816, Japan

(Received 3 March 1995)

The lifetimes of positrons in an edge dislocation, a jog, and vacancies, which are associated with the edge dislocation (associated vacancy), in bcc iron are calculated. The structures of the defects are obtained by static relaxation using the Finnis-Sinclair potential. The positron lifetimes are calculated using the superimposed-atom method, which was developed by Puska and Nieminen. The positrons are not localized strongly in the pure edge dislocation and the jog. The lifetimes in them are almost the same, and are only a few picoseconds longer than in the matrix. The vacancy is trapped on the edge-dislocation line, and is not collapsed completely by the strain in the core region of the dislocation. The positron lifetime in the associated vacancy is shorter than that in a vacancy in the matrix, and is compared to the experimental value observed in deformed iron. These results indicate that the deeper trap associated with the dislocation line is not the jog but the vacancy.

I. INTRODUCTION

Positron-annihilation-lifetime measurements have been made to investigate the behavior of lattice defects. This technique brings its ability into full play in the study of open-structured defects, such as atomic vacancies and microvoids.¹⁻⁴ When sufficient amounts of these defects exist, the positron wave function is localized in them. The positron lifetime in these defects is longer than in a perfect lattice, because the overlap of a positron and electrons in these defects is smaller than in a perfect lattice. The lifetime becomes longer up to a saturated value when the microvoid in which the positron is trapped grows larger.^{5,6}

On the other hand, the interactions between positrons and non-open-structured defects such as loops, stacking fault tetrahedra (SFT), and various dislocations have also been studied.⁷⁻¹⁶ It is generally considered that the positron lifetime in these defects is between that in a vacancy and that in a perfect lattice, because the atomic density at the core of them is slightly lower than in the surrounding region. There is, however, another opinion that a kind of interstitial loop can trap the long-lived positrons.⁸

Arponen *et al.*⁹ assumed that the positron lifetime observed in a deformed metal is due to a dislocation line. This assumption means there is a strong interaction between the positron and the dislocation. Shirai *et al.*¹⁰ measured the positron lifetimes in some metals and alloys which contain only a given type of dislocation, and found a close relation between the lifetime and the magnitude of the Burgers vector. They concluded that this result suggests the predominant trapping of positrons by the dislocation core.

On the contrary, Doyama and Cotterill¹¹ and Smedskjaer *et al.*¹² proposed the shallow trap model for dislocations. According to them, the positron binding energy in a pure straight dislocation line is small, and the positron is detrapped to the bulk or is trapped further into defects associated with the dislocation line. Häkkinen *et al.*^{13,14} calculated the positron states in the core region of pure edge dislocation and in the defects (vacancy and jog) associated with the edge dislocation in Al and Cu. Their results showed that the positron binding of the pure edge dislocation is weak, and the lifetime in it is almost the same as that in the perfect crystal. Their results for the jog and the vacancy associated with the edge-dislocation line indicated that the lifetimes in these defects are almost the same each other and have a medium value between that in the matrix and that in a single (isolated) vacancy. Hidalgo *et al.*¹⁶ measured the positron lifetime in a deformed iron, and found the lifetime to be 150 ps. Their discussion suggested that the positrons annihilate at associated defects rather than at the dislocation line.

In this paper we give the results of calculations of the positron lifetimes in a jog and vacancies associated with the edge-dislocation line (associated vacancy) in iron. In Sec. II we calculate statically the stable configurations of atoms around the edge dislocation with and without a point defect by using the Finnis-Sinclair (FS) potential.¹⁷ Consequently, no significant open space in which the positron might be bound is found in the structures around the edge-dislocation core and the jog in iron. The vacancy on the edge-dislocation line in iron does not collapse. Next, in Sec. III we calculate the positron lifetimes in the defect structures obtained above. The method to calculate the positron states here has been developed by Puska and Nieminen,⁶ and gives reliable lifetime values. The results show that the lifetimes in

the pure edge dislocation and in the jog are almost the same in iron. The lifetime in the associated vacancy is shorter than in a single vacancy in the perfect lattice and fairly longer than in a matrix. Section IV contains our conclusions.

II. STABLE CONFIGURATION OF DEFECTS

A. Method of calculation

The lattice relaxation around a defect is calculated using the FS potential.¹⁷ The FS potential is an empirical many-body potential which has been obtained on the basis of density functional theorem, and is similar to the EAM (embedded atom method) potential.¹⁸ In the FS potential the total energy U_{tot} of the model crystal consists of two terms:

$$U_{\text{tot}} = U_N + U_P, \quad (1)$$

where U_N is the *many-body* term and U_P is the *pair* term. U_N is written as

$$U_N = -A \sum_i \sqrt{\sum_{j(\neq i)} \phi(R_{ij})}, \quad (2)$$

where R_{ij} is the distance between the i th atom and the j th atom and

$$\phi(R) = \begin{cases} (R-d)^2 + \beta(R-d)^3/d, & R \leq d \\ 0, & R > d, \end{cases} \quad (3)$$

for iron. The pair potential term U_P is written as

$$U_P = \frac{1}{2} \sum_{ij} V_P(R_{ij}), \quad (4)$$

where

$$V_P(R) = \begin{cases} (R-c)^2(c_0 + c_1R + c_2R^2), & R \leq c, \\ 0, & R > c. \end{cases} \quad (5)$$

In these equations, the sum over i is taken for all atoms, and the sum over j is taken for the first and the second nearest-neighbor atoms of the i th atom. The parameters (A , d , β , c , c_0 , c_1 , and c_2) in the FS potential have been determined by fitting to the actual material characters such as the lattice constant, the elastic constants, the cohesive energy, etc.¹⁷

The model lattice is constructed as large as possible, because a dislocation has a long-range strain field around it. The results obtained from model lattices which have different sizes are compared to confirm that the model crystal size does not influence the result. The relaxed and optimal lattice configurations can be obtained through the iteration of the Newton-Raphson method. This iteration process is continued until the total energy of the model crystal reaches a saturated minimum value.

B. Edge dislocation

At the beginning, the stable configuration of the pure $(a/2)[\bar{1}\bar{1}\bar{1}]$ edge dislocation in bcc iron is calculated. The size of the model crystal is $80\sqrt{2/3}b$ for the $[110]$ direction, $80b$ for the $[\bar{1}\bar{1}\bar{1}]$ direction, and $2\sqrt{2}b$ for the $[1\bar{1}\bar{2}]$ direction where $b = 2.4825 \text{ \AA}$ is the magnitude of the Burgers vector. The numbers of the (110) , $(\bar{1}\bar{1}\bar{1})$, and $(1\bar{1}\bar{2})$ planes are 80, 240, and 6, respectively. The number of the atoms contained in this crystal is 19 200. The initial $(a/2)[\bar{1}\bar{1}\bar{1}]$ edge-dislocation line parallel to the $[1\bar{1}\bar{2}]$ direction is introduced at the center of the model crystal by displacing the atoms according to the elasticity theory. The periodic boundary condition for the $[1\bar{1}\bar{2}]$ direction and the fixed boundary conditions at the two (110) surfaces and the two $(\bar{1}\bar{1}\bar{1})$ surfaces are employed. The stable configuration is obtained after 3000 steps of the iteration process.

In the similar way, we obtain another crystal in which the edge-dislocation line is displaced toward the $[\bar{1}\bar{1}\bar{0}]$ direction by one atomic plane distance ($= \sqrt{2/3}b$). For the sake of convenience, we define "assembly I" as the *relaxed original* crystal and "assembly II" as the *relaxed* crystal in which the dislocation line is *displaced*; i.e., the dislocation line in assembly II lies on the slip plane downward adjacent to that for the dislocation line in assembly I. The difference of the total energy between these two crystals is $< 0.001 \text{ eV}$ at the final state.

The structure of the edge dislocation is represented by the density distribution $\rho(x)$ of the Burgers vector which is defined (assuming x axis parallel to the $[\bar{1}\bar{1}\bar{1}]$ direction) as

$$\rho(x) = \frac{d(\Delta u)}{dx}, \quad (6)$$

where Δu is the displacement difference between the atoms in the adjacent (110) planes above and below the slip plane. The $\rho(x)$ in both assembly I and assembly II is plotted in Fig. 1, which shows that the structures of these

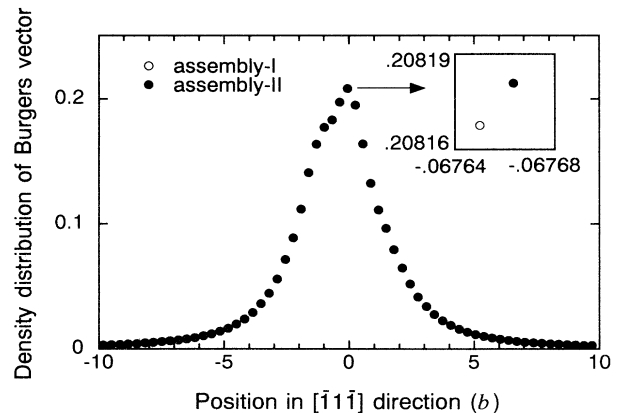


FIG. 1. The density distribution of the Burgers vector in assembly I (open circles) and in assembly II (solid circles). The difference between them is small enough (see the magnification of the peak point) to be neglected. The smaller model which contains 14 700 atoms has almost the same distribution within the accuracy of $10^{-4}b$.

two dislocations are almost the same; therefore these two dislocations can be dealt with equivalently. The similar simulation for the smaller model crystal (whose size is $70\sqrt{2/3}b$ for the $[110]$ direction and $70b$ for the $[\bar{1}\bar{1}\bar{1}]$ direction, and 14 700 atoms are contained in it) is also performed. The smaller model also has almost the same dislocation structure as the larger ones. This indicates that the size of the model crystal is large enough to obtain the structure of the edge dislocation.

C. Jog on the edge-dislocation line

To prepare the initial model crystal which includes a jog, all assemblies I and II (see Sec. IIB) were stacked toward the $[\bar{1}\bar{1}\bar{2}]$ direction in the sequence of . . . I I I II II II . . ., resulting in a crystal which has a jog at the joint of assembly I and assembly II. The size of the calculated region is $40\sqrt{2/3}b$ for the $[110]$ direction, $40b$ for the $[\bar{1}\bar{1}\bar{1}]$ direction, and $28\sqrt{2}b$ for the $[\bar{1}\bar{1}\bar{2}]$ direction. The jog is centered in this region. The numbers of the (110) , $(\bar{1}\bar{1}\bar{1})$, and $(\bar{1}\bar{1}\bar{2})$ planes are 40, 120, and 84, respectively. This region contains 67 200 atoms. Fixed boundary conditions at the surfaces of the calculated region are employed. The stable configuration is obtained after 200 steps of the iteration process.

The structure of the jog is shown in Fig. 2, which illustrates the (110) plane lying between two adjacent slip planes separated by one atomic plane distance. We divide the atomic plane into two regions as explained in the figure. The jog is positioned at the center of the figure; therefore the dislocation line lies *over* this atomic plane in region I and *under* this plane in region II. The density of atom in region I is lower than in the perfect lattice because this region is in the expansion side of the edge dislocation. Region II is included in the compression side, and the density of atoms in this region is higher than in the perfect lattice.

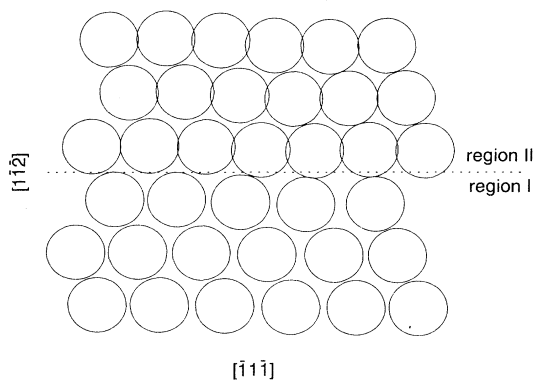


FIG. 2. The structure of the jog in iron. This plane is divided into two regions by the dotted line. Region I is included in the expansion side of the dislocation, and region II is included in the compression side. The (110) atomic plane which includes the edge of the extra half plane of the edge dislocation in region II is illustrated. This atomic plane is between the two different slip planes. The radius of the circles is half of the distance ($= b/2$) between nearest neighbors in the perfect lattice.

D. Associated vacancy on the dislocation line

The initial model crystal which contains an associated vacancy on the edge-dislocation line is obtained as follows. All assemblies I (see Sec. IIB) were stacked toward the $[\bar{1}\bar{1}\bar{2}]$ direction, resulting in a crystal which consists of 80 $(\bar{1}\bar{1}\bar{2})$ planes. And then an atom is removed to make a vacancy. The vacancy is located always on the slip plane (in the compression side), and the distance between the vacancy and the dislocation line is varied for the purpose of studying the vacancy trap on the edge dislocation. The size of the calculated region is $40\sqrt{2/3}b$ for the $[110]$ direction, $40b$ for the $[\bar{1}\bar{1}\bar{1}]$ direction, and $(80\sqrt{2/3})b$ for the $[\bar{1}\bar{1}\bar{2}]$ direction. The dislocation line penetrates the center of this region. The numbers of the (110) , $(\bar{1}\bar{1}\bar{1})$, and $(\bar{1}\bar{1}\bar{2})$ directions are 40, 120, and 80, respectively. This region contains 64 000 atoms. Fixed boundary conditions at the surface of the calculated region are employed. The calculations are iterated 200–1400 times in each case of the vacancy position to optimize the configuration.

The vacancy formation energy E_v^f is defined as

$$E_v^f = U_{d+v}^{\text{tot}} - U_d^{\text{tot}} - E^c, \quad (7)$$

where U_{d+v}^{tot} and U_d^{tot} are the total energy of the crystal which includes the edge dislocation, with and without the vacancy, respectively. $E^c = 4.28$ eV is the cohesive energy. The variation in E_v^f versus the vacancy position is plotted in Fig. 3, which indicates that the vacancy is trapped by the edge dislocation. Since the vacancy formation energy in the perfect lattice is 1.83 eV and that on the edge-dislocation line is 0.91 eV, the vacancy trapping energy of the edge dislocation is

$$E_v^f(\text{perfect}) - E_v^f(\text{on dislocation}) = 0.92 \text{ eV}. \quad (8)$$

The structures of the vacancy in the matrix and on the edge dislocation line are shown in Fig. 4. The distance between the two neighboring atoms existing on the opposite sides of the vacancy in the $[\bar{1}\bar{1}\bar{1}]$ atomic row is

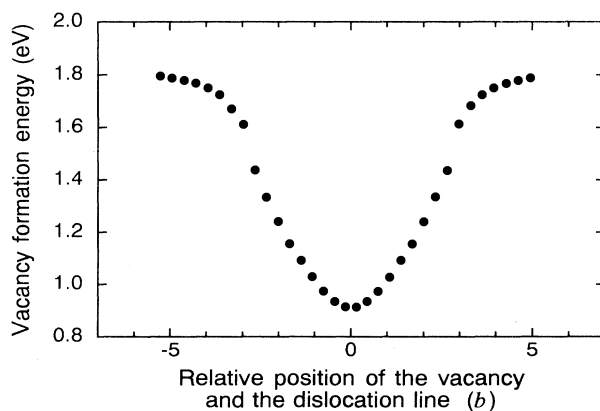


FIG. 3. The vacancy formation energy E_v^f around the edge dislocation in iron. The abscissa is the position of the atomic site to be a vacancy, measured from the dislocation line in the unit of the magnitude of the Burgers vector. The positive value in the abscissa means that the vacancy is positioned in the $[\bar{1}\bar{1}\bar{1}]$ direction of the dislocation line.

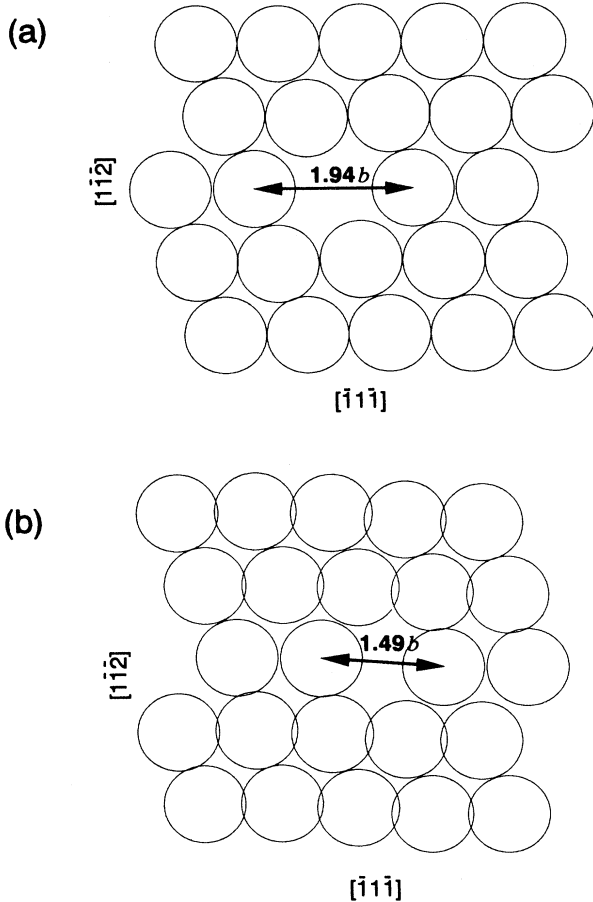


FIG. 4. The structure of (a) the isolated vacancy and (b) the associated vacancy (on the edge-dislocation line). The radius of the circles is half of the distance ($= b/2$) between nearest neighbors in the perfect lattice.

$1.94b$ in the matrix (if the lattice relaxation is not taken into consideration, this value is $2b$). In the case of the vacancy on the dislocation core, this distance is reduced to be $1.49b$ because of the large strain in the core region.

III. POSITRON LIFETIME CALCULATION

A. Method of calculation

The positron lifetimes in the defects described in Sec. II are calculated according to the method of Puska and Nieminen.⁶ This method gives a reliable positron lifetime value. The electron density distribution $n_-(\mathbf{r})$ in a crystal is approximated by superimposing the spherical averaged charge densities $n_{\text{at}}(\mathbf{r})$ (r is the distance from the atomic center) of an isolated atom:¹⁹

$$n_-(\mathbf{r}) = \sum_i n_{\text{at}}(|\mathbf{r} - \mathbf{R}_i|), \quad (9)$$

where \mathbf{R}_i is the position at which the i th atom is placed. The Coulomb potential $V_C(\mathbf{r})$ is, therefore, represented

by superimposing the function $V_{\text{at}}(r)$ of distance r from an atom:

$$V_C(\mathbf{r}) = \sum_i V_{\text{at}}(|\mathbf{r} - \mathbf{R}_i|). \quad (10)$$

The correlation potential $V_{\text{corr}}(n_-(\mathbf{r}))$ which is due to the interaction between the positron and the host electrons is represented as the function of the local electron density, based on the local density approximation. The practical form of the function $V_{\text{corr}}(n)$ has been determined by Boroński and Nieminen.²⁰ The total potential felt by a positron is

$$V(\mathbf{r}) = V_C(\mathbf{r}) + V_{\text{corr}}(n_-(\mathbf{r})). \quad (11)$$

The positron wave function $\psi_+(\mathbf{r})$ as the numerical solution of the Schrödinger equation can be obtained through the iteration process of the Kimball-Shortley method,²¹ in which the Schrödinger equation is solved at the nodes of the three-dimensional mesh. The boundary conditions and the separations of each mesh point are varied depending on the defect in question, and are described later. The energy eigenvalue of the positron wave function is obtained every iteration, and this process is continued until the eigenvalue reaches a saturated minimum value.

The positron annihilation rate λ which is the inverse of the positron lifetime τ is obtained by

$$\lambda = \pi r_0^2 c \int d\mathbf{r} n_+(\mathbf{r}) [n_v(\mathbf{r})\Gamma_v(n_v(\mathbf{r})) + n_c(\mathbf{r})\Gamma_c + n_d(\mathbf{r})\Gamma_d], \quad (12)$$

where $n_+ = \psi_+^2$ is the density of the positron, and n_v , n_c , and n_d represent the density of valence, core, and d electrons, respectively. r_0 is the classical electron radius, and c is the light velocity. Γ_v , Γ_c , and Γ_d are the enhancement factors corresponding to each electron due to the positron-electron correlation effects. According to Brandt and Reinheimer²²

$$\Gamma_v(n_v) = 1 + \frac{r_v^3 + 10}{6}, \quad (13)$$

where $r_v = (3/4\pi n_v)^{1/3}$ is the density parameter of the valence electrons. For core electrons, Γ_c has been estimated as 1.5 by Bonderup *et al.*²³ We determined the constant value for Γ_d so that the calculated lifetime in the matrix agrees with the experimental result. When we set the $\Gamma_d = 2.20$, the matrix lifetime 110 ps is reproduced in iron.²⁴

The size of the region for the calculation of the positron lifetime in the edge dislocation is $6a$ for the $[110]$ and $[\bar{1}\bar{1}\bar{1}]$ directions and $2\sqrt{2}b = \sqrt{6}a$ for the $[1\bar{1}\bar{2}]$ direction where $a = 2.8665 \text{ \AA}$ is the lattice constant. The dislocation line penetrates the center of the $(1\bar{1}\bar{2})$ surface of this region. The mesh spacing is $\sqrt{6}a/30$ for the $[1\bar{1}\bar{2}]$ direction and $a/10$ for the other two directions. Vanishing boundary conditions at the two (110) surfaces and the two $(\bar{1}\bar{1}\bar{1})$ surfaces and the periodic boundary condition for the $[1\bar{1}\bar{2}]$ direction are employed.

The calculation of the positron lifetime in the jog is

carried out in the cubic region which has the sides parallel to the $[110]$, $[\bar{1}\bar{1}\bar{1}]$, and $[1\bar{1}\bar{2}]$ directions, and the length of each side is $6a$. The jog is placed at the center of this region. The mesh spacing is $a/10$ for the three directions. The vanishing boundary conditions are imposed at the six surfaces of this region.

When the positron lifetime in the vacancy is calculated, the length of each side of the calculated region is $5a$. The vacancy is placed at the center of this region. Any other conditions are same as the case of the jog.

B. Results of lifetime calculation and discussion

The positron lifetimes obtained from the present calculations are summarized in Table I, and are discussed in this section.

The positron wave function around the edge-dislocation line is shown in Fig. 5. The boundary conditions are imposed at the frames of the figures. The wave function has the maximum value at the dislocation core and extends to the boundary region, indicating the weak trapping of the positron. If the boundary conditions are imposed at the further place, the wave function extends more. Since the positron lifetime tends to become shorter when the wave function is delocalized in the lattice, this calculation gives the upper limit of the positron lifetime. The calculated lifetime $\tau_d = 117$ ps (Table I) in the dislocation core is longer than in the perfect lattice by only 7 ps. To confirm that the result is independent of the size of the calculated region, a varied side length of the calculated region is attempted: When the lengths along the $[110]$ and $[\bar{1}\bar{1}\bar{1}]$ directions are varied like as $4a$ - $5a$ - $6a$, the lifetime gets shorter within a variation of only 1 ps. In all cases, the experimental long lifetime (150 ps) observed in the deformed iron¹⁶ cannot be due to the dislocation line.

The positron wave function in the jog is shown in Fig. 6, which illustrates the same (110) plane as Fig. 2. The jog is located at the center of this figure. The positron is weakly localized in the jog, and extends to the boundary. This situation is similar to the case of the pure edge dislocation. The calculated lifetime 117 ps in the jog is almost the same as that on the edge-dislocation line. Häkkinen *et al.*^{13,14} calculated the positron lifetime in the jog in aluminum. Their result was that the lifetime

TABLE I. The calculated positron lifetimes τ_{cal} and the experimental values τ_{exp} in iron.

Annihilation site	τ_{cal} (ps)	τ_{exp} (ps)
perfect lattice	110 ^a	110 ^b
vacancy in the matrix	181 ^c	175 ^b
edge dislocation line	117	
jog on the edge dislocation line	117	
vacancy on the edge dislocation line	140	150 ^d

^aFitted value.

^bReferences 1 and 2.

^cReference 25.

^dReference 16.

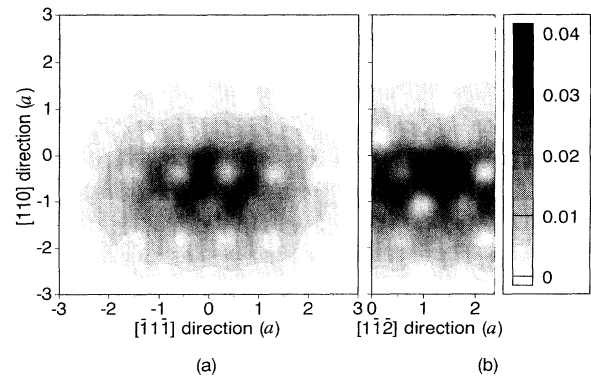


FIG. 5. The positron wave function around the edge-dislocation line in iron. (a) is the section between the two adjacent $(1\bar{1}\bar{2})$ planes, and (b) is the $(\bar{1}\bar{1}\bar{1})$ section which includes the dislocation line. The boundary conditions are imposed at the frames of these figures.

in the jog was fairly longer than on the edge dislocation and was almost the same as that in the vacancy on the dislocation. Their way of forming the jog resulted in a row of vacancies along the dislocation, because a few vacancies on the dislocation line in fcc aluminum could not be relaxed enough to be a pair of jogs. Accordingly they obtained almost the same lifetime for the jog as for the associated vacancy.¹³ In the present calculation, the jog is formed without vacancies and its configuration is realistic.

The positron wave functions in the isolated or associated vacancies are shown in Fig. 7 which illustrates the (110) plane including the vacancy. The vacancy is positioned at the center of the figures. The positron is localized in each vacancy better than in the pure edge dislocation and in the jog. The positron in the associated vacancy is localized in a smaller region than in the isolated vacancy, because the neighboring atoms of the

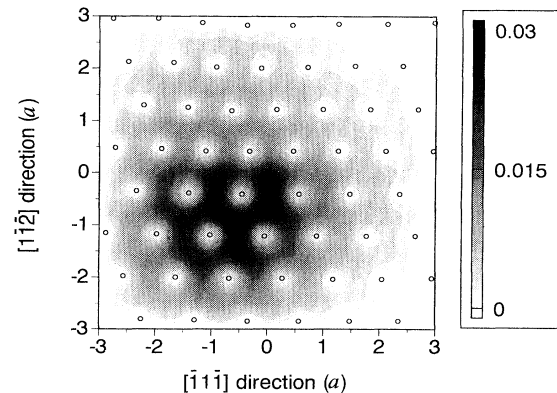


FIG. 6. The positron wave function in the jog of the edge-dislocation line in iron. The same (110) section as Fig. 2 is shown. The vanishing boundary conditions are imposed at the frame of this figure. The circles are positioned at the atomic positions.

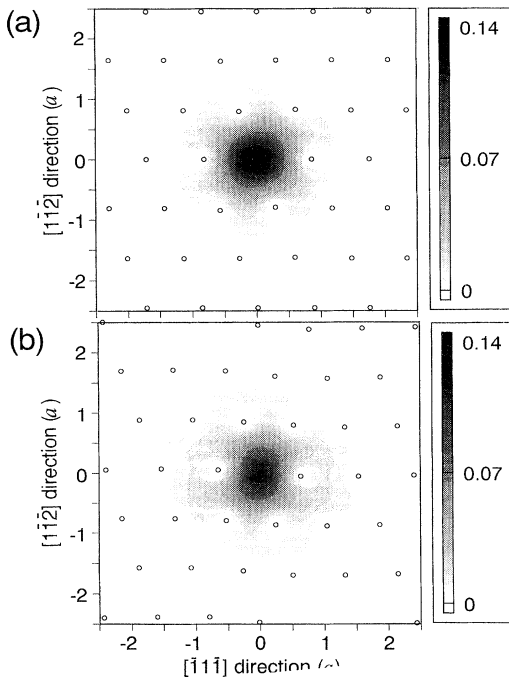


FIG. 7. The positron wave function (a) in the isolated vacancy and (b) in the associated vacancy (on the edge-dislocation line) in iron. The same (110) section as Fig. 4 is shown. The vanishing boundary conditions are imposed at the frames of these figures. The circles are positioned at the atomic positions.

vacancy are relaxed inward by the large strain in the dislocation core region. Furthermore, since the overlap integral of the density distributions of the positron and the electrons is larger in the associated vacancy than in the isolated vacancy, the positron lifetime becomes shorter in the associated vacancy. The calculated positron lifetimes are plotted in Fig. 8 as a function of the relative position of the vacancy and the dislocation line. The lifetime decreases when the vacancy gets close to the dislocation, and is 140 ps when the vacancy is completely trapped on the dislocation. There are two local minima of the positron lifetime at the position of the vacancy, $\sim \pm 2.6b$. The dislocation-pinning force by the vacancy becomes maximum at these points. (The vacancy formation energy around the dislocation shown in Fig. 3 can be also interpreted as the interaction potential between the edge-dislocation line and the vacancy. The maxima of the gradient of this potential are seen at these points in Fig. 3, indicating the maxima of the pinning force at

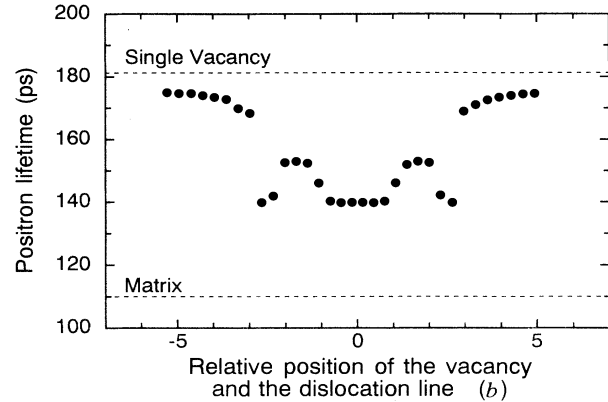


FIG. 8. The calculated positron lifetime versus the position of vacancy. The calculated results for the perfect lattice (matrix) and for the vacancy in the matrix are also shown. The abscissa is the same as Fig. 3.

these points.) This large pinning force causes the large strain around the defects, and suppresses the vacancy volume. This is the reason for the local minima of the positron lifetime. The lifetimes in the associated vacancy near the dislocation line are compared to the experimental lifetime (150 ps) observed in deformed iron.¹⁶ The associated vacancy is, therefore, the first candidate defect for the deep trap of the positron.

IV. CONCLUSIONS

We calculated the stable configuration of an edge dislocation, a jog, and vacancies associated with the dislocation line in iron. The dislocation line and the jog do not have any significant open space in their structures. The vacancy trapped on the dislocation line is not collapsed completely, and still remains the open volume. The vacancy trapping energy of the edge-dislocation line is 0.92 eV.

We also calculated the positron lifetimes in these defects in iron. The positron is weakly localized in the edge-dislocation core and the jog, and the lifetimes in them are almost the same as each other, that is, 117 ps. The positron lifetime in the associated vacancy is 140 ps, which is compared to the experimental value observed in deformed iron. These results support the shallow trap model of the edge dislocation, and show that the deeper trap is not the jog but the vacancy associated with the edge-dislocation line.

¹ P. Hautojärvi *et al.*, *Solid State Commun.* **29**, 855 (1979).

² A. Vehanen, P. Hautojärvi, J. Johansson, and J. Yli-Kauppila, *Phys. Rev. B* **25**, 762 (1982).

³ E. Kuramoto *et al.*, *Mater. Sci. Forum* **105-110**, 1125 (1992).

⁴ C. Corbel and P. Moser, in *Proceedings of Yamada Conference V on Point Defect and Defect Interactions in Metals, Kyoto, 1981*, edited by J. Takamura, M. Doyama, and

M. Kiritani (University of Tokyo Press, Tokyo, 1981), p. 445.

⁵ P. Hautojärvi, J. Heinö, M. Manninen, and R. Nieminen, *Philos. Mag.* **35**, 973 (1977).

⁶ M. J. Puska and R. M. Nieminen, *J. Phys. F* **13**, 333 (1983).

⁷ E. Kuramoto, Y. Aono, M. Takenaka, and K. Kitajima, *J. Phys. Soc. Jpn.* **52**, 1098 (1983).

⁸ W. Frank, A. Seeger, and M. Weller, in *Proceedings of*

- the 6th International Conference on Positron Annihilation, The University of Texas at Arlington, 1982*, edited by P. G. Coleman, S. C. Sharma, and L. M. Diana (North-Holland, Amsterdam, 1982), p. 413.
- ⁹ J. Arponen, P. Hautojärvi, R. Nieminen, and E. Pajanne, *J. Phys. F* **3**, 2092 (1973).
- ¹⁰ Y. Shirai, K. Matsumoto, G. Kawaguchi, and M. Yamaguchi, *Mater. Sci. Forum* **105-110**, 1225 (1992).
- ¹¹ M. Doyama and R. M. J. Cotterill, in *Proceedings of the 5th International Conference on Positron Annihilation, Lake Yamanaka, 1979*, edited by R. R. Hasiguti and F. Fujiwara (Japan Institute of Metals, Aoba Aramaki, Sendai, 1979), p. 89.
- ¹² L. C. Smedskjaer, M. Manninen, and M. J. Fluss, *J. Phys. F* **10**, 2237 (1980).
- ¹³ H. Häkkinen, S. Mäkinen, and M. Manninen, *Europhys. Lett.* **9**, 809 (1989).
- ¹⁴ H. Häkkinen, S. Mäkinen, and M. Manninen, *Phys. Rev. B* **41**, 12441 (1990).
- ¹⁵ Y. K. Park *et al.*, *Phys. Rev. B* **34**, 823 (1986).
- ¹⁶ C. Hidalgo, G. González-Doncel, S. Linderoth, and J. S. Juan, *Phys. Rev. B* **45**, 7017 (1992).
- ¹⁷ M. W. Finnis and J. E. Sinclair, *Philos. Mag. A* **50**, 45 (1984).
- ¹⁸ M. S. Daw and M. I. Baskes, *Phys. Rev. B* **29**, 6443 (1984).
- ¹⁹ F. Herman and S. Skillman, *Atomic Structure Calculations* (Prentice-Hall, Englewood Cliffs, NJ, 1963).
- ²⁰ E. Boroński and R. M. Nieminen, *Phys. Rev. B* **34**, 3820 (1986).
- ²¹ G. E. Kimball and G. H. Shortley, *Phys. Rev.* **45**, 815 (1934).
- ²² W. Brandt and J. Reinheimer, *Phys. Lett.* **35A**, 109 (1971).
- ²³ E. Bonderup, J. U. Andersen, and D. N. Lowy, *Phys. Rev. B* **20**, 883 (1979).
- ²⁴ Y. Kamimura, F. Hori, T. Tsutsumi, and E. Kuramoto, *Trans. Mater. Res. Soc. Jpn.* **16A**, 385 (1994).
- ²⁵ Y. Kamimura, F. Hori, T. Tsutsumi, and E. Kuramoto, *Mater. Sci. Forum.* **175-178**, 403 (1995).

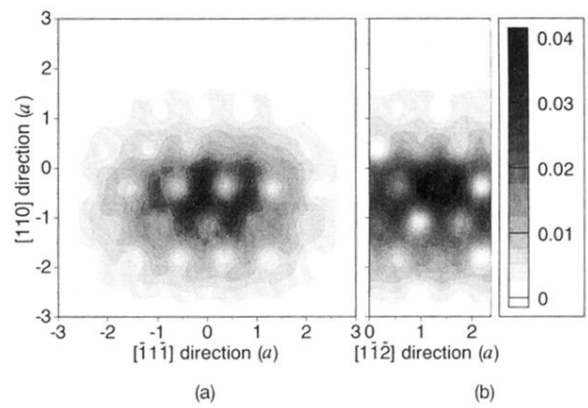


FIG. 5. The positron wave function around the edge-dislocation line in iron. (a) is the section between the two adjacent $(\bar{1}\bar{1}\bar{2})$ planes, and (b) is the $(\bar{1}\bar{1}\bar{1})$ section which includes the dislocation line. The boundary conditions are imposed at the frames of these figures.

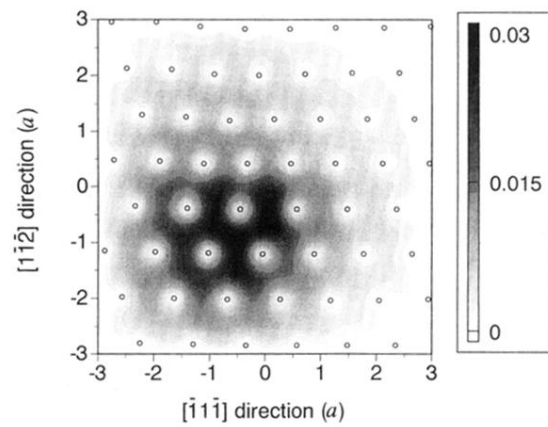


FIG. 6. The positron wave function in the jog of the edge-dislocation line in iron. The same (110) section as Fig. 2 is shown. The vanishing boundary conditions are imposed at the frame of this figure. The circles are positioned at the atomic positions.

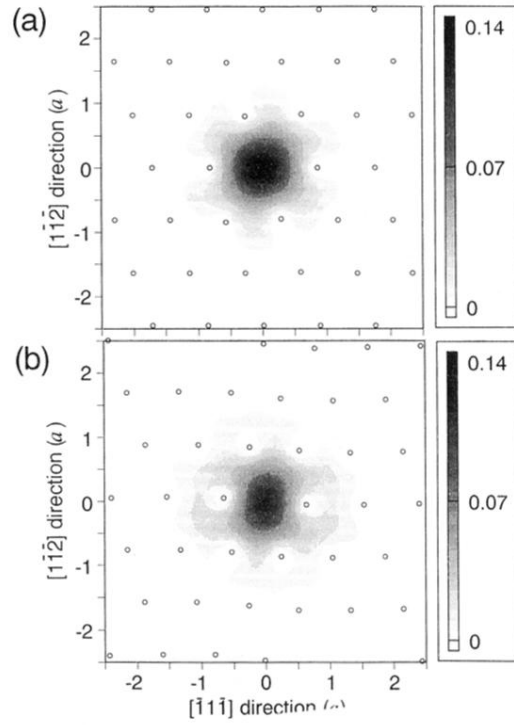


FIG. 7. The positron wave function (a) in the isolated vacancy and (b) in the associated vacancy (on the edge-dislocation line) in iron. The same (110) section as Fig. 4 is shown. The vanishing boundary conditions are imposed at the frames of these figures. The circles are positioned at the atomic positions.